# Representation of interval timing by temporally scalable firing patterns in rat prefrontal cortex

Min Xu[a,1], Si-yu Zhang[a,1], Yang Dan[b], and Mu-ming Poo[a,2]

[a]Institute of Neuroscience, State Key Laboratory of Neuroscience, Shanghai Institutes for Biological Sciences, Chinese Academy of Sciences, Shanghai 200031, China; and [b]Division of Neurobiology, Department of Molecular and Cell Biology, Helen Wills Neuroscience Institute, Howard Hughes Medical Institute, University of California, Berkeley, CA 94720

Contributed by Mu-ming Poo, November 24, 2013 (sent for review June 17, 2013)

**Perception of time interval on the order of seconds is an essential component of cognition, but the underlying neural mechanism remains largely unknown. In rats trained to estimate time intervals, we found that many neurons in the medial prefrontal cortex (PFC) exhibited sustained spiking activity with diverse temporal profiles of firing-rate modulation during the time-estimation period. Interestingly, in tasks involving different intervals, each neuron exhibited firing-rate modulation with the same profile that was temporally scaled by a factor linearly proportional to the instructed intervals. The behavioral variability across trials within each task also correlated with the intertrial variability of the temporal scaling factor. Local cooling of the medial PFC, which affects neural circuit dynamics, significantly delayed behavioral responses. Thus, PFC neuronal activity contributes to time perception, and temporally scalable firing-rate modulation may reflect a general mechanism for neural representation of interval timing.**

Perception of time on the order of seconds (interval timing) is crucial for a variety of behaviors (1–4). In interval timing-related tasks, the animal must keep track of the elapsed time from a previous event and decide when to anticipate a future event or to execute motor actions. Whereas timing perception in shorter timescale (e.g., motor timing) is controlled by automatic timing system in the cerebellum (5, 6), interval timing is thought to involve prefrontal and parietal cortices (7), which are associated with attention and working memory (8). However, how timing information is represented in the neural activity in these cortical areas is unclear. To understand how the brain performs time estimation, it would be particularly useful to examine changes in the pattern of neuronal activity when the animal estimates different time intervals. We thus designed a behavioral task in which the rat was required to estimate two time intervals in the same behavioral session, and multiple single-unit recording was performed concurrently to examine how the task timing was represented by activities of medial prefrontal cortex (mPFC) neurons. Finally, local brain cooling was applied to explore whether mPFC neural network dynamics play causal role in the animal's perception of time intervals on the order of seconds.

## Results

Adult rats were trained to perform the time-estimation task (Fig. 1*A* and Movie S1), with two instructed durations (1.5 and 2.5 s) in alternating blocks of trials. Each trial was initiated when the rat poked the nose into the waiting port. After a random delay (drawn from a uniform distribution within 0.5–1.5 s), a sound stimulus was presented to indicate the instructed duration of either 1.5 s (pure tone) or 2.5 s (white noise). During "instructive trials," the sound was presented for the instructed duration, and the rat was rewarded only if it exited from the waiting port within a ~1-s window (*Materials and Methods*) at the sound termination. The "exit time" is defined as the time between sound onset and the rat exit from the waiting port. During a "test trial" (randomly interleaved with instructive trial in each block), the sound stimulus was prolonged for 1 s (Fig. 1*A*), but the rat was rewarded only if it exited the waiting port within the same window as that used in the instructive trials. Thus, in these test trials the rat must estimate the elapsed time from the sound onset to receive the reward, because the delayed sound offset no longer served as the exit signal. In the example session illustrated by Fig. 1 *B* and *C*, we found that the exit times in instructive trials exhibited symmetric distributions centering around the instructive duration for both the 1.5- and 2.5-s blocks (1.5-s block: 1.62 ± 0.27 s; 2.5-s block: 2.59 ± 0.32 s), whereas the exit times in test trials for both blocks showed similar distributions and mean values (1.5-s block: 1.69 ± 0.30 s; 2.5-s block: 2.60 ± 0.37 s). The exit times for both instructive and test trials were slightly longer than the instructive sound durations (1.5 and 2.5 s). This may be attributed to the animal's reaction time and the asymmetric position of the reward window relative to the instructive sound offset. To summarize all data from four rats in 77 sessions, we plotted the mean values of exit times for the distributions of instructive and test trials from each session (arrows in Fig. 1 *B* and *C*). As shown in Fig. 1 *D* and *E*, the mean exit times during test trials were significantly longer than those of instructive trials for both 1.5-s (1.75 ± 0.26 s, test trials; 1.65 ± 0.17 s, instructed trials; $P < 0.001$; paired *t* test) and 2.5-s task (2.62 ± 0.24 s, test trials; 2.50 ± 0.19 s, instructed trials; $P < 0.001$; paired *t* test). These results indicate that the rats could reliably perform time-estimation tasks for two different durations in the same test session.

Several models have been proposed for interval timing, including pacemaker-accumulator model (1, 9, 10) and coincidence detection of oscillatory processes (11). To explore the neural mechanism underlying interval timing behavior, we performed chronic single-unit recording in the mPFC, a structure known to be critical for working memory (12) and interval-timing discrimination (13–15) in rats. During the time-estimation task,

### Significance

**The ability to estimate time interval in the order of seconds is important for animal behaviors. However, how the brain estimates the passage of time remains mysterious. In the current study, we trained rats to estimate two different time intervals and recorded activities of single neurons from the medial prefrontal cortex (mPFC). We found that some PFC neurons showed activity changes during time estimation by the rat, with the same profile that was temporally scaled by a factor proportional to the estimated time intervals. Local cooling of mPFC slowed the time estimated by the rat. Thus, PFC neuronal activity contributes to time estimation, and temporal scaling of neuronal activity may be a circuit mechanism for estimating different time intervals.**

Author contributions: M.X., Y.D., and M.-m.P. designed research; M.X. and S.-y.Z. performed research; M.X. analyzed data; and M.X., Y.D., and M.-m.P. wrote the paper.

The authors declare no conflict of interest.

[1]Present address: Department of Molecular and Cell Biology, University of California, Berkeley, CA 94720.

[2]To whom correspondence should be addressed. E-mail: mpoo@ion.ac.cn.

This article contains supporting information online at www.pnas.org/lookup/suppl/doi:10.1073/pnas.1321314111/-/DCSupplemental.

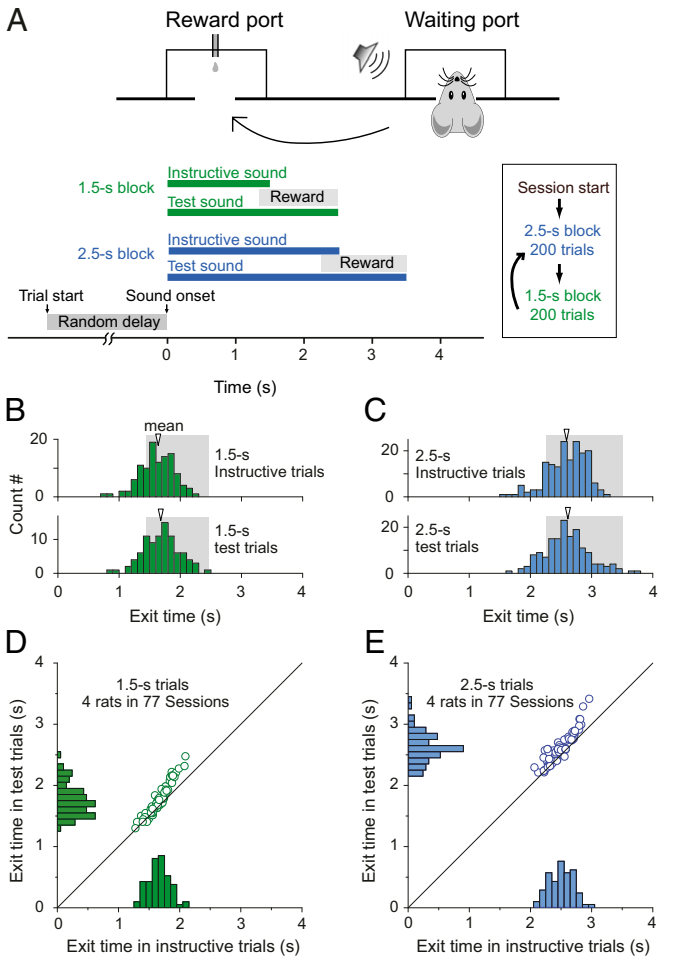


**Fig. 1.** Two-duration time-estimation task. (*A*) Schematic diagrams for the behavioral tasks. To initiate a trial, the rat poked its nose into the waiting port and held it at the port for a pseudorandom delay of 0.5–1.5 s before the sound signal was given. In instructive trials, a standard sound (of 1.5- or 2.5-s duration) was played. Rats were rewarded with a small drop of water delivered in the reward port only when they exited from the waiting port within the reward window (from 0.15 or 0.25 s before to 1 s after the sound offset for the 1.5- and 2.5-s tasks, respectively) and then poked into the reward port immediately after exit. During test trials, which were randomly interleaved with instructive trials in each session, a prolonged sound was played and reward was given only if the rat exited the waiting port within the same reward window as in the instructed trials. (*B*) Performance from one experimental session in 1.5-s instructive trials and test trials. The histogram shows distribution of exit times. Shadow area indicates the reward window. (*C*) Performance of the same rat in the same experimental session as shown in *B* in 2.5-s blocks. (*D* and *E*) Performance of four rats in the two-interval time-estimation task. Histograms and scatter plots show the distribution of mean exit time from four rats in 77 sessions (13–30 sessions per rat) of performing the two-duration timing task. The bin size in all histograms is 100 ms.

mPFC neurons exhibited a wide variety of firing patterns (Fig. 2) that were associated with different phases of the task. Fig. 2 shows the firing patterns from three example neurons, with the activities aligned by the time of waiting port entry, sound onset, or waiting port exit respectively. The neuron shown in Fig. 2*A* exhibited distinct peaks at waiting port entry and exit time, whereas the neuron in Fig. 2*B* showed sustained firing following the initial firing-rate increase at waiting port entry, indicating mPFC neurons firing could encode multiple aspects of the behavior. Beside these neurons showing activities primarily correlated with the movements during the task, we observed neurons (Fig. 2*C*) that exhibited sustained firing during the period between the sound onset and waiting port exit (referred to hereafter as "time-estimation period"), which might contribute to the time-estimation behavior of the animal.

To identify neural activities that are related to time-estimation behavior, we focused our analysis on neurons that exhibited significant modulation of firing rates during the time-estimation period of test trials, as defined by significant difference ($P < 0.05$, one-way ANOVA) in firing rates over three consecutive nonoverlapping periods (0.7 s each, from 0.2 to 2.3 s from the sound onset) for all 2.5-s test trials of each session (*Materials and Methods*). We found that the majority of mPFC neurons (64%, 247/389) showed firing-rate modulation during the time-estimation period. Among these neurons, 30% (75/247; *Materials and Methods*) showed monotonic activity increase, 35% (86/247) showed monotonic decrease, and 35% (86/247) showed nonmonotonic changes. Fig. 3 *A* and *B* depicts the spiking activity of an example neuron in 25 consecutive test trials. For both the 1.5-s and 2.5-s time-estimation tasks, the firing rates (aligned by the sound onset; *Materials and Methods*) exhibited a sudden decrease when the rat entered the waiting port and a gradual increase during the time-estimation period, reaching similar levels when the rat exited from the waiting port. Interestingly, the rate of increase was slower for the 2.5-s task (Fig. 3*B*), and the activity profile matched closely with that of 1.5-s task when we temporally compressed the 2.5-s peri-stimulus time histogram (PSTH) profile by a factor of 0.65 (red dashed line in Fig. 3*A*), the ratio between mean exit times for the two tasks. Fig. 3*C* depicts different activity profiles observed during the time-estimation period for three other example neurons, exhibiting monotonic increase or decrease, or nonmonotonic changes before reaching the same exit activity level for both timing tasks. Again, the firing profiles for each neuron during 1.5-s and 2.5-s tasks closely resembled each other and matched well after temporally scaling the 2.5-s profile by a factor of ~0.65 (exit time ratio between 1.5-s and 2.5-s tasks).

To quantify the temporal scaling property across the neuronal population, we calculated the best temporal scaling factor that yielded the minimum difference between PSTHs of the two timing tasks during the time-estimation period (Fig. 3*D* and *Materials and Methods*). As shown in Figs. 2 and 3*C*, the firing pattern of many neurons exhibited close correlation with port

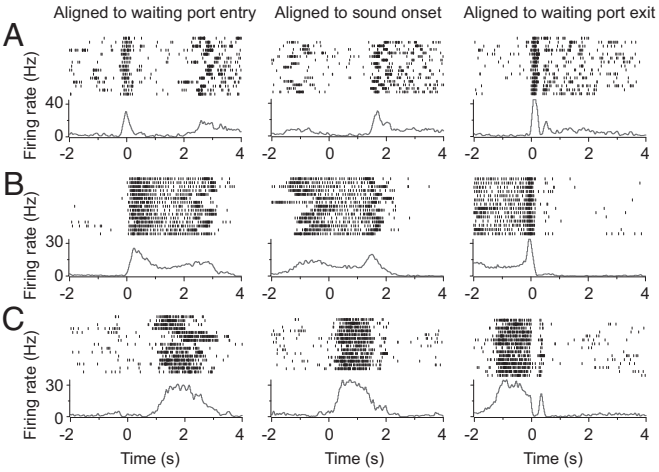


**Fig. 2.** Spiking activities of three neurons (*A–C*) in mPFC during the task. (*A–C*, *Upper*) Raster plots of spiking activity for 15 consecutive trials, with each row corresponding to one trial (tick mark, single spike) and the time aligned by the time of waiting port entry (*Left*), sound onset (*Center*), or waiting port exit (*Right*), respectively. (*A–C*, *Lower*) PSTH from the same session as the raster plot.

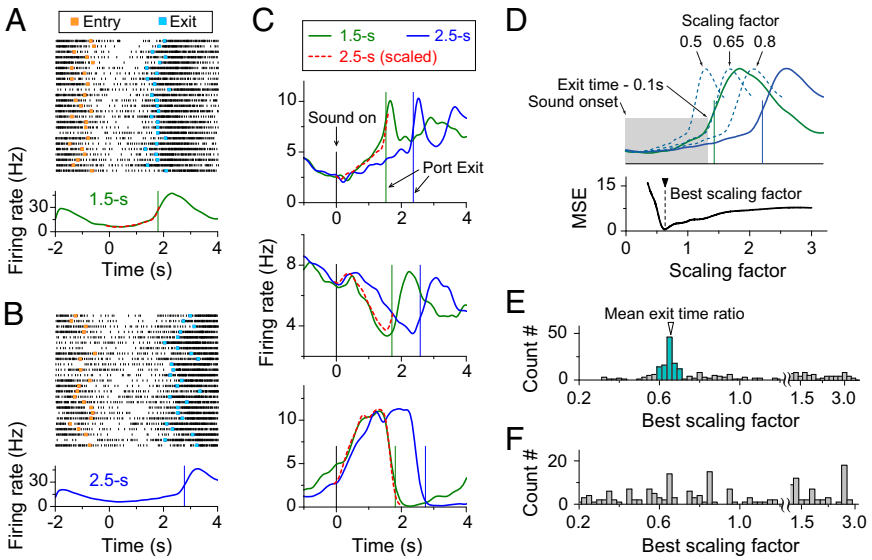


**Fig. 3.** Temporal scaling of firing patterns in mPFC neurons. (*A*) Example of spiking activity of one mPFC neuron in a rat performing 1.5-s trials. (*A*, *Upper*) The raster plot of spiking activity for 25 consecutive trials, with each row corresponding to one trial (tick mark: single spike). Trials are aligned by the sound-onset time (zero). (Orange squares, port-entry time; cyan squares, port-exit time.) (*A*, *Lower*) PSTH (*Materials and Methods*) from the same session as the raster plot. The green curve shows the PSTH of neural activity in 1.5-s test trials, and the red dashed curve is the temporally scaled PSTH of 2.5-s test trials. The green vertical line shows the mean exit time. (*B*) Example of neural activity from the same neuron as shown in *A* during the same experimental session in 2.5-s test trials. (*C*) Examples of neuron showing the temporally scalable activity during time-estimation period. The green curve is PSTH of neural activity in 1.5-s test trials, and the blue curve is PSTH of neural activity in 2.5-s test trials. The red dashed curve is PSTH of neural activity in 2.5-s test trials scaled by the ratio between the mean exit times in 1.5-s test trials and that in 2.5-s test trials. Green vertical line, the mean exit time in 1.5-s test trials; blue vertical line, the mean exit time in the 2.5-s test trials. (*D*) Calculation of the best scaling factor, based on the minimum MSEs (*Materials and Methods*). (*E*) Distribution of the best scaling factor during time-estimation period (*Materials and Methods*); 45% (111/247) of the best scaling factors fell within ±10% from the mean exit-time ratio of 0.67 (colored histogram). (*F*) Distribution of best scaling factor during the random-delay period from two-interval time-estimation task. Data consist of 247 neurons from 77 behavioral sessions of four rats.

entry and exit. To reduce potential interference by these movement-related activities when calculating the best scaling factor, we excluded the immediate 100-ms period before waiting port exit (Fig. 3*D*). The distribution of best scaling factors for 247 neurons in four rats showed a distinct peak at ∼0.65, (Fig. 3*E*), and 111 neurons have their scaling factors fell within ±10% from the mean exit time ratio 0.67 (range: 0.6–0.74). Thus, 28% (111/389) of the recorded neurons, or 45% (111/247) of neurons showing temporally modulated firing during the time-estimation period, appeared to show temporal scaling of their activity profile in accordance with the task timing during the two-interval time-estimation task. Finally, to examine whether the temporal scaling applied only to the time-estimation period or to all periods between the 1.5- and 2.5-s blocks, we performed the same temporal-scaling analysis on the activity during the "random-delay period" (from waiting port entry to the sound onset; *Materials and Methods*). We found that the scaling factors exhibited no distinct peak (Fig. 3*F*), indicating that temporal scaling by the ratio of exit times is specific to the activity during the time-estimation period. This temporal scalability suggests that the activity profile during time-estimation period carries task timing information, consistent with the finding in PFC neurons of monkeys performing a working memory task (16).

To further test the idea that PFC neuronal activity during the time-estimate period contributes to the time-estimation behavior of the rat, we examine whether the firing patterns of individual neurons are directly related to the intertrial variability of exit times. We divided all of the 2.5-s test trials within each block into the early- and late-exit groups by the median exit time. As shown in Fig. 4 *A* and *B* for two example neurons, PFC neural activity showed faster rate modulation in the early- than late-exit group ($P = 0.025$; paired $t$ test; *Materials and Methods*), and temporal scaling by the ratio of mean exit times of the two groups resulted in closely matched activity profiles. For all of the 247 neurons examined, the distribution of best scaling factors for the early- and late-exit groups peaked at ∼0.8, which is close to the ratio of mean exit times for the two groups, and 83% (206/247) of the scaling factors fell within ±5% from the mean exit time ratio 0.81 (range: 0.77–0.86; Fig. 4*C*). We further divided the 2.5-s test trials into eight groups based on the exit times and found that the distribution of best scaling factors showed linear correlation with the ratio of the mean exit times of these groups (scaling of the latter seven groups relative to the first group; Fig. 4*D*). Thus, intertrial variability in the dynamics of mPFC firing patterns during the time-estimation period could contribute directly to the variability in the rat's time-estimation behavior.

To directly test the causal role of mPFC neuronal activity in the rat's time-estimation behavior, we manipulated the mPFC neuronal activity by local cooling (Fig. 5*A* and Fig. S1). Compared with pharmacological manipulations, the local cooling method allows fast and reversible switching between normal and slowed neural temporal dynamics (17–19). Calibration of the cooling device in anesthetized rats showed that the local brain temperature drop was linearly related to the cooling current (Fig. 5*A*). At a cooling current of 600 mA, the temperature dropped by 7 °C within 10 s at a distance of ∼250 μm from the cooling probe, and it reversed with a similar time constant when the cooling current was terminated (Fig. 5*A*). The rats exhibited no obvious behavioral change during the period of the moderate local cooling used in these experiments. We then applied the cooling treatment to the mPFC of both hemispheres (Fig. 5*B*) during the rat's performance of the 2.5-s time-estimation task, with 100-s cooling interleaved with 100-s noncooling periods. We found that cooling significantly prolonged the exit time, as shown by the cumulative percentage plot of exit times from one example session (Fig. 5*B*; $P = 0.024$; Kolmogorov–Smirnov test) and the summary of 55 sessions from

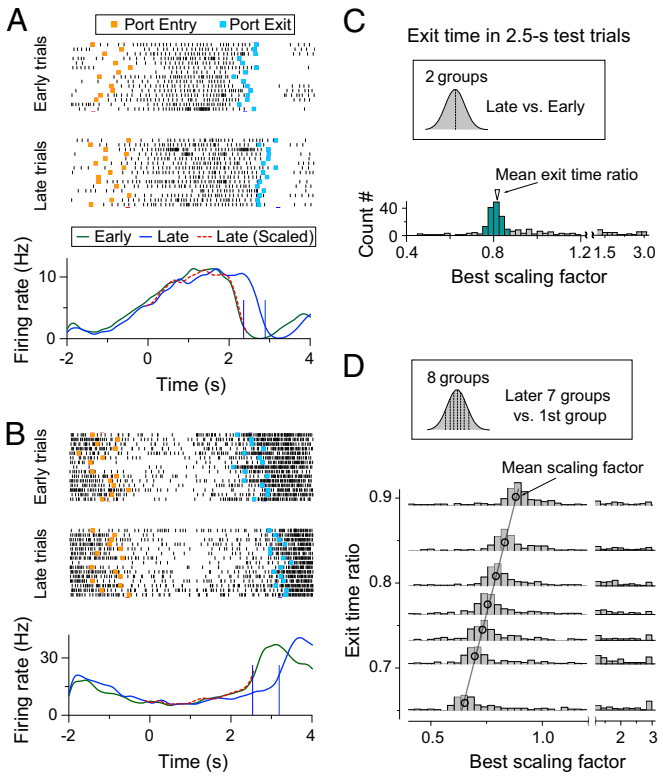


**Fig. 4.** Behavioral variability and temporal scaling of neural activity in mPFC. (*A* and *B*) Two examples of neural activity in 2.5-s test trials. Trials are grouped based on the exit times into the early-exit group and late-exit group. (*A* and *B*, *Top* and *Middle*) Raster plots of spiking activity in early-exit (*Top*) and late-exit (*Middle*) trials separately are shown. (Orange squares, port-entry time; cyan squares, port-exit time.) (*A* and *B*, *Bottom*) The green and blue curves depict PSTH of early- and late-exit trials, respectively, and the red dashed curve represents temporally scaled PSTH of the late-exit trials. (*C*) Distribution of the best scaling factor between early- and late-exit trials in 2.5-s testing trials (*Materials and Methods*); 83% (206/247) of the scaling factors fell within ±5% from the mean exit time ratio 0.81 (colored histogram). Data consist of 247 neurons from 77 behavioral sessions of four rats. (*D*) Correlation between exit-time ratios and best scaling factors. Trails were divided into eight groups according the exit-time values, with the same number of trials in each group. Histograms show the distribution of best scaling factor between seven later exit groups and the first fastest exit group. Black circles mark the value of mean exit-time ratio and best scaling factor, both determined by the Gaussian fit of individual distributions. Black line, best linear fit of the black circles ($r^2 = 0.99$).

six rats (Fig. 5*B*; $P = 0.0029$; paired $t$ test). The cooling effect on exit times was not attributable to general slowing of rat's movements, because we found no significant change in the time for the rat to move from the waiting port to the reward port between the cooling and no-cooling periods (Fig. S2; $P = 0.82$; paired $t$ test). Also, this effect was specific to the mPFC, because the same cooling treatment applied to the adjacent motor cortices had no effect on exit times (Fig. 5*B*; $P = 0.64$; paired $t$ test). These results support the idea that mPFC neuronal dynamics contributes to the time-estimation behavior.

## Discussion

In the present study, we have examined whether and how neuronal activity in the mPFC represents interval timing in two-interval time-estimation task. We found that 28% of the recorded mPFC neurons exhibited temporal scaling of their activity profiles during the time-estimation period in accordance with the task timing. Two lines of evidence suggest that these mPFC neurons play an active role in interval-timing behavior of the rat. First, the intertrial variability of the time estimation, as reflected by the waiting port-exit time, correlates strongly with the variability of the activity profiles of these neurons. Second, altering the neuronal dynamics in the mPFC by local cooling prolonged the perceived time, as shown by the delayed waiting port exit, during the time-estimation task. These results provide a basis for further study of the neuronal mechanism underlying interval timing.

The highly diverse firing patterns of mPFC neurons we observed during the time-estimation task are consistent with those found in the PFC of both monkey (20–22) and rat (12, 15, 23–26) during the animal's performance of various behavioral tasks. This presumably reflects the heterogeneity of PFC neurons that are involved in regulating diverse aspects of each behavior. For example, we observed neurons with reproducible activity patterns that are well correlated with different phases of the task, including port entry and exit, sound onset, and reward onset, which involve regulatory actions of mPFC neurons on sensory and motor systems. Despite the diverse firing patterns of mPFC neurons, a substantial portion (28%) of them exhibited temporal scaling of their firing patterns when performing two different timing tasks, suggesting that temporally scalable firing-rate modulation may serve as a mechanism for mPFC neurons to represent interval timing. Our finding is consistent with the model that timing information is inherent in the neural network dynamics (16, 27, 28).

Timing-related signals have been observed in neuronal activity in a variety of brain regions, including PFC (7, 29–32), lateral intraparietal area (LIP) (33, 34), presupplementary and supplementary motor areas (35), basal ganglia (32, 36, 37), cerebellum (3), and thalamus (38). In monkeys performing the time-discrimination task, the LIP neuronal activity ramps up or down at slow and fast speeds in long and short timing tasks, respectively (33), consistent with temporal scaling. Unlike the monotonic ramping activity found in LIP (33, 39) and thalamus (38), the activity of mPFC neurons we observed here exhibited more complex (sometimes nonmonotonic; Fig. 3*C*, the third neuron) temporal profiles, which could be associated with signals for movement planning (waiting port exit) or reward expectation. Although neuronal activity in many brain areas could carry time-related signals, it has been difficult to determine whether these timing signals originate from a central area where interval timing is carried out. Our evidence from local cooling studies supports the idea that PFC-related neural network may play an active role in interval timing perception. Local temperature change in the brain affects the kinetics of various ion channels, leading to changing dynamics of neural network (18, 19). In the birdsong system, local brain cooling was used to demonstrate the causal role of a brain region in controlling the song timing (17). Analogous to the native singing behavior, we found that local brain cooling could also affect a cognitively controlled learned behavior of timing perception. In this study, we showed that temporal scaling of mPFC neural activity correlates well with the rat's time-estimation behavior during the two-interval time-estimation task. Similar temporal scaling of PFC neural activity has been reported during the delay period for the working memory task in monkeys (16). In the latter task, active time estimation by the monkey may not be required, because the monkey could simply wait for the appearance of the second cue. However, similar scaling of PFC neural activity observed in both tasks indicated that temporal scaling of neuronal firing may be a general neural mechanism for coding different time intervals.

An important question is how the scaling-invariant activity profile could be achieved by neural circuits. Monotonic ramp up of the firing rate can be achieved by integration of stochastic inputs with a constant mean (28, 40) or firing-rate adaptation of inhibitory neurons (28), and the ramping speed can be controlled by the number of active inputs or the degree of adaptation of the inhibitory neurons, which can be learned through Hebbian synaptic modifications. In a recently proposed oscillator-based model of

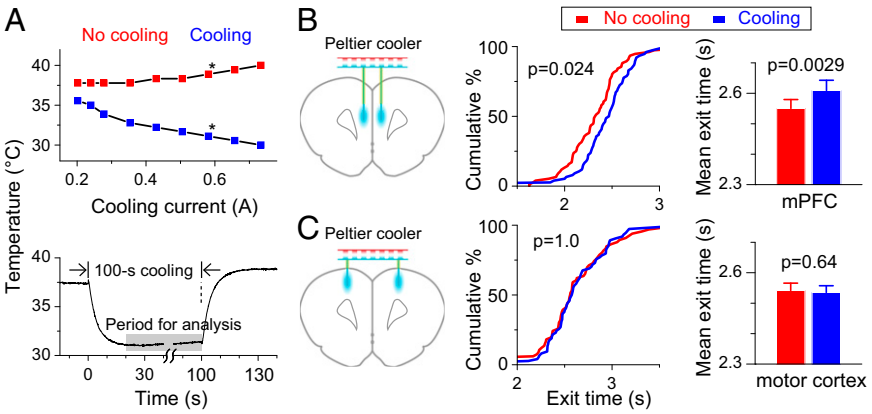


**Fig. 5.** Cooling of mPFC slows the time-estimation behavior. (*A*) Measurement of local brain cooling. (*A*, *Upper*) Temperature changes at ~250 μm from cooling probe using different cooling currents. (Blue and red squares, average data during the cooling and noncooling periods; star, cooling current used for behavioral experiments.) (*A*, *Lower*) Temperature changes following the onset and offset of the cooling current. (*B*, *Left*) Schematic diagram of the cooling device and position of cooling probes. (*B*, *Center*) Cumulative percentage plot of exit times with and without cooling for example behavioral session. (*B*, *Right*) Histograms summarizing results of mean exit times in 55 sessions from six rats. (*C*) The same cooling treatment at the motor cortices resulted in no effect on exit times. Data are from four rats in 40 sessions.

movement generation (11), a complex profile of neuronal firing in an "integrator" could result from the sum of multiple harmonics of an oscillator. The temporal scaling of the profile is controlled by the fundamental frequency of the oscillator, which is set simply by the amplitude of an external input. A future challenge is to determine whether such a model is applicable to the temporal scaling of mPFC activity reported here and what are the underlying neural circuits.

## Materials and Methods

**Animal.** Adult (>8 wk) male Sprague–Dawley rats or Long–Evans rats were used in all experiments. All experimental procedures were approved by Institute of Neuroscience, Chinese Academy of Sciences Animal Care and Use Committee.

**Two-Interval Time-Estimation Task.** The behavioral chamber contained an aluminum panel with two ports: the right port ("waiting port") for time estimation and the left port ("reward port") for water delivery (Fig. 1*A* and Movie S1). Entry and exit from ports were detected by infrared beam located inside of each port. Port signals were digitally interfaced to an RX5-2/RZ5 real-time workstation (TDT) through laboratory-built circuits. The water-delivery valve (SMC VX2120-02-5G1) was controlled by the same work station through a laboratory-built isolating board.

The behavioral task required the rat to estimate sound durations and to respond by exiting from waiting port at the right timing, followed by poking into reward port to receive water reward. During the initial stage of the training, an instructive sound with fixed duration was used to guide the rat to exit from the waiting port at the fixed time (right after the sound offset). After rats learned the initial stage of the task, one-third of the instructive sound was replaced by a prolonged sound (1 s longer) to test whether rats could use the internal time estimation to guide their behavior, because the delayed-sound offset no longer served as the exit signal. The task consisted of two alternating blocks, a 1.5-s block and a 2.5-s block (Fig. 1*A*). In the 1.5-s block, the instructive sound was 1.5-s 2-kHz pure tone, and the prolonged sound was 2.5-s 2-kHz pure tone. In the 2.5-s block, the instructive sound was 2.5-s white noise, and the prolonged sound was 3.5-s white noise.

The rats self-initiated each experimental trial by poking their snouts into the waiting port and keeping their snouts within the port (Fig. 1*A*). After a variable delay, drawn from a uniform random distribution of 0.5–1.5 s, a sound, either an instructive sound or a prolonged sound, was delivered (Fig. 1*A*) in pseudorandom order within each session. The task required rats keeping their snouts within the waiting port for at least 90% of required holding time (1.5 s or 2.5 s) according to the sound presented (white noise or 2 KHz pure tone). Rats were rewarded only when they exited the waiting port and poked into the reward port, as required by the timing of reward window (Fig. 1*A*). The reward window consisted of two successive periods: the first period was from 90% of the required holding time to the end of the holding time plus 1 s (1.35–2.5 s for the 1.5-s task; 2.25–3.5 s for the 2.5-s task), during which rats were required to exit from the waiting port; the second period was a 1.5-s window starting from the exit time, during which rats were required to poke into the reward port. If rats exited from the waiting port earlier than the minimum holding time, the training system would not respond to any poking action from the rats within 16 s, starting from the reward-port entry time (time-out period). A new trial could be triggered after 6 s (intertrial interval) from the reward-port entry time, except for the time-out trials.

**Behavior-Training Procedure.** Water-restricted rats were introduced to the training chamber, and a small drop of water was automatically given at the reward port after a 2.5-s white noise was played every 2 min. Sound play and water delivery could also be triggered if rats poked their snouts into the waiting port. After rats could reliably obtain water at the reward port by poking into the waiting port, a minimum waiting-port holding time was introduced and gradually increased from ~0.5 s to the required holding time according to individual rat's performance. When rats learned to hold their snouts in the waiting port during sound play, the random-delay period and the reward window were introduced to the training. The reward window was gradually decreased from ~10 s to the final length according to individual rat's performance. Most of the rats could learn this initial stage of the training in 2 wk. Once rats learned the first stage, the prolonged test sound was introduced, and 1 more week was usually needed for them to reach stable performances. Rats were then trained in the 1.5-s task for 1 wk before they were exposed for the final task, performing both the 2.5-s task and the 1.5-s task during the same session.

**Single-Unit Recording.** Well-trained rats were implanted with laboratory-made potentiometer-based microdrives carrying 32-channel microwire array in both hemispheres of the mPFC (centered 3.2 mm anterior to bregma and 0.5 mm lateral to midline; Fig. S3). Electrodes array consisted of thirty-two 25-μm-diameter FeNiCr wires (Stablohm 675; California Fine Wire) (41). Wires were cut with sharp scissors and electroplated with platinum (H2PtCl6; Aldrich) to an impedance of ~300 kΩ with a laboratory-built MSP430 MCU-controlled multichannel plating device. The electrode assembly was advanced by 37 or 75 μm every day to search for active cells. Neuronal activity was recorded using a TDT System-3 neurophysiology workstation (with an RA16 preamplifier + RX5 workstation, also used to record behavior data) controlled by OpenEx software (TDT). Single units were isolated manually using principle component analysis-based clustering methods. All data analysis was performed in Matlab (Mathworks) and Neuroexplorer (Nex Technologies).

**Local Brain Cooling.** For cooling experiments, rats were trained in 2.5-s timing task, and laboratory-built Peltier effect-based cooling devices were implanted to both mPFCs (3.2 mm anterior to bregma, 0.5 mm lateral to midline, and 3.0 mm from brain surface; $n = 6$ rats) or both motor cortices (3.2 mm anterior to bregma, 2.0 mm lateral to midline, and 1.0 mm from brain surface; $n = 4$ rats). The cooling device consisted of five main parts (42) (Fig. S1*A*): a thermoelectric Peltier device (Custom Thermoelectric; no. 01801-9G30-12CN) for generating the cooling; a polyimide-tubing insulated, gold-plated, sharpened silver wire (375 μm) to conduct cooling to the targeting areas; a cooper heat sink (modified from MOS-C10; Enzotech) to facilitate convection

from warm side of Peltier device; a thermocouple (Omega Engineering, 5SC-TT-K-40-36) to monitor working status of the whole device; and a connector for all wires ($4 \times 36$ gauge wires) carrying supply current and thermocouple output signal. The heat sink and cooling probe were soldered onto the Peltier device using Bismuth-tin solder (Custom Thermoelectric) and sealed with silicone elastomer (KwikCast; WPI). The cooling device was powered by a modified, constant-current light-emitting diode driver (Luxdrive 3021-D-E-1000) to generate bidirectional currents. The amplitude and polarity of the current were controlled by a TDT RZ5 real-time workstation. Amplitude of the current used in the experiment was 600 mA for the cooling period and −200 mA for the no-cooling period to compensate the temperature drop by convection, which was determined by calibrating the cooling device in the anesthetized animal (Fig. 5*A*). The cooling protocol was 100-s cooling periods, separated by 100-s no-cooling periods. Approximately 7 °C of cooling was induced at ∼250 μm away from the cooling probe (Fig. 5*A*).

**Data Analysis.** To measure behavior performance, we generated PSTH for exit times, which were the durations from the sound onset to the time of the rat's exit from the waiting port. The bin size for behavior PSTH was 100 ms. All port entry and exit times were extracted off-line using Matlab from the recorded port signal. An exit-time histogram was fitted using Gaussian function, ($y = y0 + Ae^{-(x-x0)^2/2\sigma^2}$), in Matlab to determine the mean exit time ($x_0$) and exit-time variation ($|\sigma|$). To extract time estimation-related behavior, we excluded trials in which rats exited too early or too late. The range of exit time used in all analysis was 1.0–2.5 s for the 1.5-s block and 1.8–3.5 s for the 2.5-s block, which included the majority of the trials (90.9% in the 1.5-s block and 91.8% in the 2.5-s block).

PSTH for spiking activity in an individual trial was constructed using 10-ms bins. PSTHs of individual trials were firstly aligned by sound-onset time and then linearly scaled to the mean exit time to generate average PSTH for each group to remove the variability introduced by variation in exit time. To test the modulation during time-estimation period, we chose three consecutive nonoverlapping periods (0.7 s each, from 0.2 to 2.3 s from the sound onset) for all 2.5-s test trials and tested the firing rate difference using one-way ANOVA. Neurons with $P < 0.05$ in the statistic test were considered to be significantly modulated during time-estimation period. The mean firing rates of the three nonoverlapping periods (0.7 s each, from 0.2 to 2.3 s from the sound onset) were used to determine the modulation profile (monatomic increase, monatomic decrease, or nonmonatomic changes) during the time-estimation period. To determine the best scaling factor (the scaling factor given the minimum difference after scaling) between the 1.5-s block and the 2.5-s block, we linearly compressed the PSTH of the 2.5-s block using different scaling factors (∼0.3–3; the low boundary was determined by sample length) and calculated the mean-squared error (MSE) to the PSTH of the 1.5-s block using the following equation (Fig. 3*D*):

$$MSE(f) = \frac{1}{n}\sum_{i=1}^{n}\left[PSTH_{1.5}(t_i) - PSTH_{2.5}(f * t_i)\right]^2,$$

and the $f$ that gave the minimum MSE was taken as the best scaling factor. To examine whether the temporal scaling applied only to the time-estimation period or to all periods between the 1.5- and 2.5-s blocks, neural activity from the random-delay period was divided into two groups according to whether they were belonged to the 1.5-s block or the 2.5-s block, and the best scaling factors were calculated between the two groups. To test temporal scaling within the same block, trials from the 2.5-s block were divided into "early-exit" and "late-exit" groups, based on whether the exit time was shorter or longer than the median exit time, respectively, and best scaling factors were calculated between the two groups (Fig. 4*C*). All statistical tests were performed in OriginLab.

**ACKNOWLEDGMENTS.** We thank Drs. Long-nian Lin and Michael Fee for advice on chronic recording and brain-cooling methods. This work was supported by grants from the Ministry of Science and Technology (973 Program Grant 2011CBA00400) and the Chinese Academy of Sciences (Strategic Priority Research Program Grant XDB02020001).

1. Buhusi CV, Meck WH (2005) What makes us tick? Functional and neural mechanisms of interval timing. *Nat Rev Neurosci* 6(10):755–765.
2. Gibbon J, Malapani C, Dale CL, Gallistel C (1997) Toward a neurobiology of temporal cognition: Advances and challenges. *Curr Opin Neurobiol* 7(2):170–184.
3. Ivry RB, Spencer RM (2004) The neural representation of time. *Curr Opin Neurobiol* 14(2):225–232.
4. Mauk MD, Buonomano DV (2004) The neural basis of temporal processing. *Annu Rev Neurosci* 27:307–340.
5. Buonomano DV, Karmarkar UR (2002) How do we tell time? *Neuroscientist* 8(1): 42–51.
6. Ivry RB (1996) The representation of temporal information in perception and motor control. *Curr Opin Neurobiol* 6(6):851–857.
7. Duncan J (2001) An adaptive coding model of neural function in prefrontal cortex. *Nat Rev Neurosci* 2(11):820–829.
8. Lewis PA, Miall RC (2003) Distinct systems for automatic and cognitively controlled time measurement: Evidence from neuroimaging. *Curr Opin Neurobiol* 13(2):250–255.
9. Gibbon J (1977) Scalar expectancy theory and Weber's law in animal timing. *Psychol Rev* 84(3):279–325.
10. Treisman M (1963) Temporal discrimination and the indifference interval. Implications for a model of the "internal clock" *Psychol Monogr* 77(13):1–31.
11. Matell MS, Meck WH (2004) Cortico-striatal circuits and interval timing: Coincidence detection of oscillatory processes. *Brain Res Cogn Brain Res* 21(2):139–170.
12. Baeg EH, et al. (2003) Dynamics of population code for working memory in the prefrontal cortex. *Neuron* 40(1):177–188.
13. Dietrich A, Allen JD (1998) Functional dissociation of the prefrontal cortex and the hippocampus in timing behavior. *Behav Neurosci* 112(5):1043–1047.
14. Kim J, Jung AH, Byun J, Jo S, Jung MW (2009) Inactivation of medial prefrontal cortex impairs time interval discrimination in rats. *Front Behav Neurosci* 3:38.
15. Narayanan NS, Laubach M (2006) Top-down control of motor cortex ensembles by dorsomedial prefrontal cortex. *Neuron* 52(5):921–931.
16. Brody CD, Hernández A, Zainos A, Romo R (2003) Timing and neural encoding of somatosensory parametric working memory in macaque prefrontal cortex. *Cereb Cortex* 13(11):1196–1207.
17. Long MA, Fee MS (2008) Using temperature to analyse temporal dynamics in the songbird motor pathway. *Nature* 456(7219):189–194.
18. Volgushev M, Vidyasagar TR, Chistiakova M, Eysel UT (2000) Synaptic transmission in the neocortex during reversible cooling. *Neuroscience* 98(1):9–22.
19. Volgushev M, Vidyasagar TR, Chistiakova M, Yousef T, Eysel UT (2000) Membrane properties and spike generation in rat visual cortical cells during reversible cooling. *J Physiol* 522(Pt 1):59–76.
20. Freedman DJ, Riesenhuber M, Poggio T, Miller EK (2001) Categorical representation of visual stimuli in the primate prefrontal cortex. *Science* 291(5502):312–316.
21. Nieder A, Freedman DJ, Miller EK (2002) Representation of the quantity of visual items in the primate prefrontal cortex. *Science* 297(5587):1708–1711.
22. Wallis JD, Anderson KC, Miller EK (2001) Single neurons in prefrontal cortex encode abstract rules. *Nature* 411(6840):953–956.
23. Gallagher M, McMahan RW, Schoenbaum G (1999) Orbitofrontal cortex and representation of incentive value in associative learning. *J Neurosci* 19(15):6610–6614.
24. Kepecs A, Uchida N, Zariwala HA, Mainen ZF (2008) Neural correlates, computation and behavioural impact of decision confidence. *Nature* 455(7210):227–231.
25. Mainen ZF, Kepecs A (2009) Neural representation of behavioral outcomes in the orbitofrontal cortex. *Curr Opin Neurobiol* 19(1):84–91.
26. Schoenbaum G, Chiba AA, Gallagher M (1999) Neural encoding in orbitofrontal cortex and basolateral amygdala during olfactory discrimination learning. *J Neurosci* 19(5):1876–1884.
27. Ivry RB, Schlerf JE (2008) Dedicated and intrinsic models of time perception. *Trends Cogn Sci* 12(7):273–280.
28. Reutimann J, Yakovlev V, Fusi S, Senn W (2004) Climbing neuronal activity as an event-based cortical representation of time. *J Neurosci* 24(13):3295–3303.
29. Genovesio A, Tsujimoto S, Wise SP (2006) Neuronal activity related to elapsed time in prefrontal cortex. *J Neurophysiol* 95(5):3281–3285.
30. Niki H, Watanabe M (1979) Prefrontal and cingulate unit activity during timing behavior in the monkey. *Brain Res* 171(2):213–224.
31. Oshio K, Chiba A, Inase M (2006) Delay period activity of monkey prefrontal neurones during duration-discrimination task. *Eur J Neurosci* 23(10):2779–2790.
32. Rao SM, Mayer AR, Harrington DL (2001) The evolution of brain activation during temporal processing. *Nat Neurosci* 4(3):317–323.
33. Leon MI, Shadlen MN (2003) Representation of time by neurons in the posterior parietal cortex of the macaque. *Neuron* 38(2):317–327.
34. Janssen P, Shadlen MN (2005) A representation of the hazard rate of elapsed time in macaque area LIP. *Nat Neurosci* 8(2):234–241.
35. Mita A, Mushiake H, Shima K, Matsuzaka Y, Tanji J (2009) Interval time coding by neurons in the presupplementary and supplementary motor areas. *Nat Neurosci* 12(4):502–507.
36. Matell MS, Meck WH, Nicolelis MA (2003) Interval timing and the encoding of signal duration by ensembles of cortical and striatal neurons. *Behav Neurosci* 117(4):760–773.
37. Meck WH, Penney TB, Pouthas V (2008) Cortico-striatal representation of time in animals and humans. *Curr Opin Neurobiol* 18(2):145–152.
38. Komura Y, et al. (2001) Retrospective and prospective coding for predicted reward in the sensory thalamus. *Nature* 412(6846):546–549.
39. Maimon G, Assad JA (2006) A cognitive signal for the proactive timing of action in macaque LIP. *Nat Neurosci* 9(7):948–955.
40. Simen P, Balci F, de Souza L, Cohen JD, Holmes P (2011) A model of interval timing by neural integration. *J Neurosci* 31(25):9238–9253.
41. Schoenbaum G (2001) *Methods in Chemosensory Research*, eds Nicolelis MAL, Simon SA (CRC, Boca Raton, FL), pp 371–427.
42. Aronov D, Fee MS (2011) Analyzing the dynamics of brain circuits with temperature: design and implementation of a miniature thermoelectric device. *J Neurosci Methods* 197(1):32–47.